

# 1 Measurements of $t\bar{t}H$ and $tH$ associated production at 2 CMS

---

3 **Sergio Sánchez Cruz<sup>a,b,\*</sup> (on behalf of the CMS Collaboration)**

4 <sup>a</sup>*Universidad de Oviedo (formerly),*  
5 *Oviedo, Spain*

6 <sup>b</sup>*University of Zurich,*  
7 *Zurich, Switzerland*

8 *E-mail: [sergio.sanchez.cruz@cern.ch](mailto:sergio.sanchez.cruz@cern.ch)*

We present measurements of the  $t\bar{t}H$  and  $tH$  associated production rate performed by the CMS  
Collaboration in a sample of pp collision events at  $\sqrt{s} = 13$  TeV. The analyses are performed  
in the diphoton and multilepton channels by categorizing events according to the lepton and  
9 jet multiplicity, and to multivariate classifiers that discriminate signals from the corresponding  
background processes. The observed results are consistent with the SM expectations, achieving  
sensitivities close to five standard deviations with respect to the background-only hypothesis for  
 $t\bar{t}H$  production.

*40th International Conference on High Energy physics - ICHEP2020*  
*July 28 - August 6, 2020*  
*Prague, Czech Republic (virtual meeting)*

---

\*Speaker

## 1. Introduction

The discovery of the Higgs (H) boson in 2012 by the ATLAS [1] and CMS [2, 3] experiments was one of the main missing pieces to complete the Standard Model (SM) of particle physics. While the properties of the recently discovered particle resemble the expectations by the SM, their precise study remains of paramount importance.

This contribution focuses on the Yukawa interaction ( $y_t$ ) between the H boson and the top quark, the heaviest particle in the SM. Although deviations of this interaction from its SM prediction can affect the H boson production rate via gluon fusion and its decay rate into two photons, these interactions are mediated by loop diagrams, which could receive contributions from Beyond SM (BSM) particles that could mask deviations of the top quark Yukawa interaction. The  $t\bar{t}H$  and  $tH$  processes involve this coupling at tree level, so this effect cannot be present. In  $tH$  production, diagrams proportional to the Higgs coupling to the W boson ( $g_W$ ) and  $y_t$  interfere destructively in the SM. However if the sign of one of these couplings is flipped, the interference becomes constructive, enhancing the cross section of this process by an order of magnitude. Therefore the study of  $tH$  production provides sensitivity to the sign of  $y_t$ .

## 2. Measurements in the $H \rightarrow \gamma\gamma$ signatures

Despite of the low branching fraction of the Higgs boson decay into photons, diphoton signatures provide a clean final state that allows to resolve the Higgs boson system in  $t\bar{t}(H \rightarrow \gamma\gamma)$  candidate events almost without ambiguity, and with little contribution from other SM processes. A measurement of  $t\bar{t}H$  production [4] is performed in events with two photons and in categories with and without leptons, targeting the hadronic and semi-leptonic decays of the top quarks. Multivariate methods are used to discriminate between signal and backgrounds. The signal production rate is measured by performing a likelihood fit to the diphoton invariant mass, obtaining a signal strength of  $1.38_{-0.29}^{+0.36}$  and an observed (expected) significance of 6.6 (4.7) standard deviations.

## 3. Measurements in the multilepton signatures

Multilepton signatures show two or more leptons in the final state, and target decay modes of the Higgs boson into  $WW^*$ ,  $ZZ^*$  and  $\tau\tau$ , and semileptonic or hadronic decays of each one of the top quarks. These signatures are typically characterized by a moderate contribution from other SM backgrounds and signal has a significantly large branching ratio. The analysis described in this contribution is fully documented in [5].

### 3.1 Event selection

The expected signal signature are final state with multiple leptons, one (two) b jets in  $tH$  ( $t\bar{t}H$ ) events and several light jets produced in the top quark or H boson decays.  $tHq$  events additionally feature a light flavor jet that may be emitted in the forward direction, due to the presence of the spectator quark. Events in this measurement are selected and classified in ten disjoint signal regions, according to the lepton (e and  $\mu$ ) and semi-hadronically decaying  $\tau$  ( $\tau_h$ ) multiplicity:  $2lSS + 0\tau_h$ ,  $3l + 0\tau_h$ ,  $2lSS + 1\tau_h$ ,  $2lOS + 1\tau_h$ ,  $1l + 2\tau_h$ ,  $4l + 0\tau_h$ ,  $3l + 1\tau_h$ ,  $2l + 2\tau_h$ ,  $1l + 1\tau_h$  and

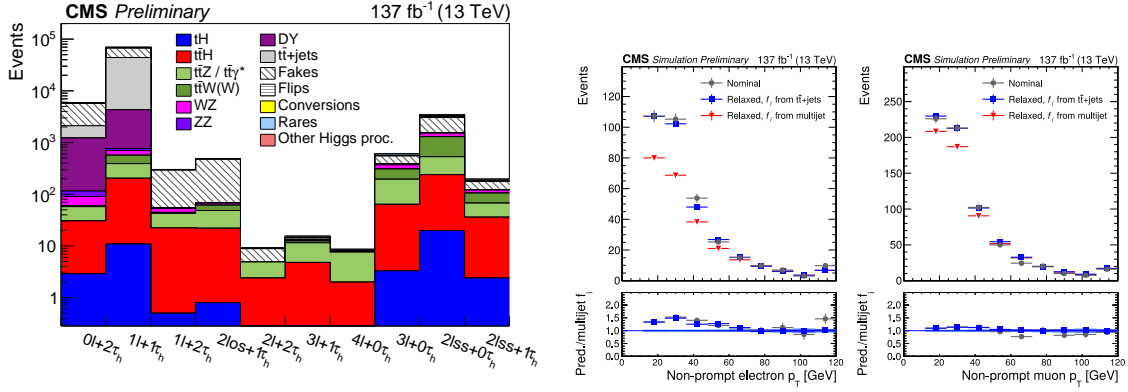


**Figure 1:** Number of expected signal and background event in each one of the signal regions (left). Transverse momentum distribution of nonprompt electrons (middle) and muons (right) in simulated  $t\bar{t}$  events. The distribution of the nominal samples (gray) is compared to the prediction of the MP method with MPs computed in  $t\bar{t}$  (blue) and multijet (red) simulated samples [5].

47  $0\ell + 2\tau_h$ . The charge of the leptons and  $\tau_h$  are required to be consistent with the expected final state  
 48 in  $t\bar{t}H$  and  $tH$  events. Additionally, in the  $2\ell SS + 0\tau_h$  category the two leptons are required to be of  
 49 the same sign, in order to profit from this rare SM topology, that enhances the signal-to-background  
 50 ratio by a large factor, while keeping roughly half of the signal dilepton events. Events are also  
 51 required to have a jet and b-tagged jet multiplicity consistent with the expected  $t\bar{t}H$  final state. This  
 52 requirement is relaxed in the  $2\ell SS + 0\tau_h$ ,  $3\ell + 0\tau_h$  and  $2\ell SS + 1\tau_h$  categories, in which sensitivity to  
 53  $tH$  production is expected, and all events with a b-tagged jet and a light (possibly forward) jet are  
 54 accepted. The signal and background contribution to the defined signal regions is shown in Fig. 1,  
 55 as obtained from the background estimation methods described in Sec. 3.2.

56 The categories defined have a significant contribution from signal events, but backgrounds  
 57 are still the dominant contribution. In order to gain sensitivity to the signals, events are classified  
 58 according to the event topology and by means of multivariate classifiers. A dedicated classifier has  
 59 been built and optimized for each category with a suitable choice of input variables. These input  
 60 variables include 3-momenta of the reconstructed objects, angular distances and invariant masses  
 61 of groups of objects, as well as multivariate discriminators aiming to reconstruct the H boson and  
 62 top quark decay products.

63 The  $2\ell SS + 0\tau_h$ ,  $3\ell + 0\tau_h$  and  $2\ell SS + 1\tau_h$  implement artificial neural networks (ANN) that aim  
 64 to classify between the different signal and background species. These ANNs feature a number  
 65 of output nodes that return a quantity that can be interpreted as the probability for an event to  
 66 have been produced by a given process. In the  $3\ell + 0\tau_h$  and  $2\ell SS + 1\tau_h$  categories the ANNs  
 67 implemented have three nodes, aiming to discriminate  $t\bar{t}H$ ,  $t\bar{t}H$  events and backgrounds, while  
 68 in the  $2\ell SS + 0\tau_h$  category the ANN employed features a fourth node, to discriminate  $t\bar{t}W$ . One  
 69 sub-category is built for each node of the ANN, containing events for which that score is the highest.  
 70 Events may then be classified according to the lepton flavor and to the b-tagged jet multiplicity.  
 71 Finally, events are classified according to the score of the most probable node.

72 The rest of the categories are not expected to profit from this multi classification approach  
 73 because they do not have enough  $tH$  contribution or they are dominated by background. In those

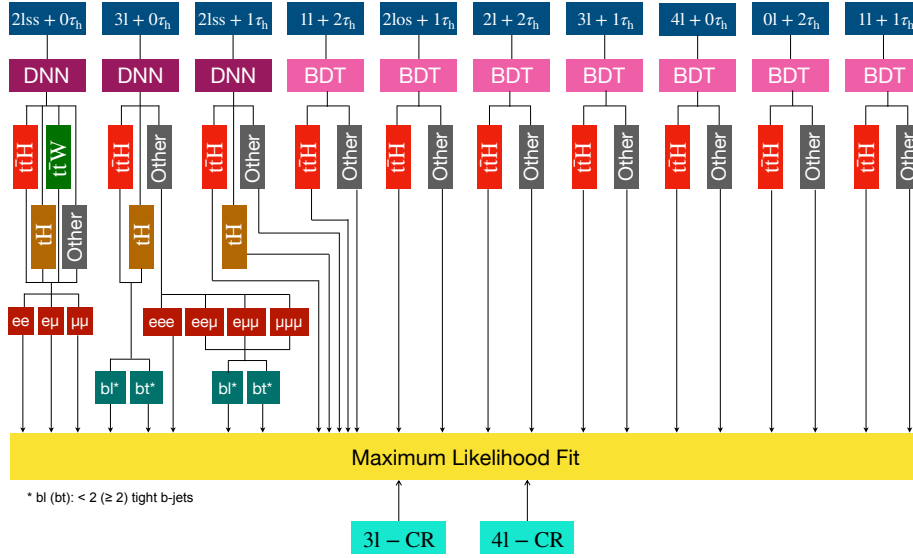


**Figure 2:** Overview of the categories used for the signal extraction [5].

74 cases, events are classified according to a boosted decision tree (BDT) that discriminates the  $t\bar{t}H$   
 75 signal from background. Figure 2 describes the categorization of events employed in the analysis.

### 76 3.2 Background estimation

77 The classification described in the previous section allows to obtain regions purer in signal  
 78 events. However, a precise background estimation remains crucial for the analysis.

79 Reducible backgrounds are dominated by the contribution from nonprompt leptons and misiden-  
 80 tified  $\tau_h$ , and electron charge flips. The contribution from these processes in the signal regions is  
 81 estimated using data driven method. There is a residual contribution from photon conversions to  
 82 electrons, that is estimated using samples of simulated events.

83 The contribution from nonprompt leptons is highly suppressed by means of an MVA discrim-  
 84 inator developed for this analysis and that makes use of impact parameter, isolation and b tagging  
 85 variables to discriminate prompt and nonprompt leptons. Misidentified  $\tau_h$  are also suppressed by  
 86 employing a selection based in the DeepTau algorithm [6]. Nonprompt leptons and misidentified  $\tau_h$   
 87 are estimated using the misidentification probability (MP) method, that infers their contribution in  
 88 the signal region from their contribution to a sideband constructed by relaxing the lepton and  $\tau_h$   
 89 selection criteria. The MP for a nonprompt lepton passing these relaxed criteria to pass the selection  
 90 on the MVA discriminator is determined from a data sample of multijet events. This is equivalently  
 91 done for misidentified  $\tau_h$  in a sample of  $t\bar{t}$ +jets events.

92 Figure 1 shows the validity of the MP method in  $t\bar{t}$  simulated events, in which their prediction  
 93 in the signal region is compared to the estimation of the MP method applied to these simulations  
 94 in the relaxed region. The method is performed with MPs computed in  $t\bar{t}$  and multijet simulated  
 95 events, separately for electrons and muons, showing a very good closure for the first ones and  
 96 acceptable for the latter ones.

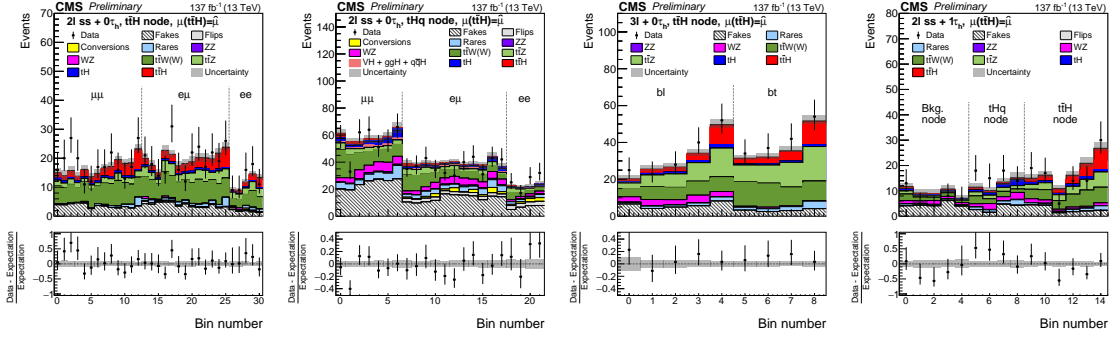


**Figure 3:** Observed events in the  $2\ell SS + 0\tau_h t\bar{t}H$  (left),  $2\ell SS + 0\tau_h tHq$  (center left),  $3\ell + 0\tau_h t\bar{t}H$  (center right) and  $2\ell SS + 1\tau_h$  (right) categories [5].

97 Electron charge flips are also estimated in a data driven way in the regions requiring two  
 98 same-sign leptons, using the opposite-sign region as a sideband. The flip rate has been determined  
 99 in a  $Z \rightarrow ee$  data sample.

100 Irreducible backgrounds are dominated by  $t\bar{t}Z$  and  $t\bar{t}W$  in the main signal regions.  $t\bar{t}Z$   
 101 and  $t\bar{t}W$  events simulated at next-to-leading-order (NLO) using the MADGRAPH5\_AMC@NLO [7]  
 102 generator. These samples are produced with one additional parton with multijet merging. The  
 103 modeling of  $t\bar{t}W$  events includes  $\alpha^3$  and  $\alpha_s\alpha^3$  electroweak corrections [8, 9], also simulated  
 104 MADGRAPH5\_AMC@NLO. Generated events are then interfaced to PYTHIA 8 citepythia to model  
 105 the parton shower, the hadronization and the underlying event. The normalization of the simulated  
 106 samples is an unconstrained nuisance parameter of the fit, allowing to constrain this quantity from  
 107 data. Two dedicated control regions are used to constrain  $t\bar{t}Z$  in events with three or four leptons  
 108 in the final state, while the contribution from  $t\bar{t}W$  is constrained from the  $t\bar{t}W$  subcategory in the  
 109  $2\ell SS + 0\tau_h$  category.

110 Other contributions from vector boson pair production or rare processes ( $t\bar{t}t\bar{t}$  or  $tZq\bar{q}$ ) are also  
 111 relevant. Top pair production and  $DY$ +jets events are irreducible in the  $1\ell + 1\tau_h$  and  $0\ell + 2\tau_h$  regions.  
 112 All these processes are simulated using simulations and normalized to the most precise cross  
 113 sections.

### 114 3.3 Results and signal extraction

115 Signals are extracted by performing a maximum likelihood fit to data in all the subcategories of  
 116 signal and control regions. This signal extraction assumes the distributions of the signal to behave  
 117 according to the SM expectations, allowing only variations of the production rate of the processes  
 118 as BSM effects. The likelihood fit implements the systematic uncertainties as nuisance parameters  
 119 of the fit. Uncertainties on the parameters of interest are estimated using a  $t$ -statistic similar to the  
 120 one employed in [11].

121 Figure 3 shows the distribution of events in some of the signal regions after the likelihood fit is  
 122 performed, showing a good compatibility between data and the fitted model. The regions enriched  
 123 in signal events also show a clear presence of the fitted  $t\bar{t}H$  signal.

124 The fitted signal strength is  $0.92 \pm 0.19$  (stat) $_{-0.13}^{+0.17}$  (syst) for the  $t\bar{t}H$  signal and  $5.7 \pm 2.7$  (stat)  $\pm$   
 125  $3.0$  (syst) for the  $tH$  signal, compatible with the SM expectations. The postfit value for the un-

126 constrained nuisance parameters that represent the  $t\bar{t}W$  and  $t\bar{t}Z$  production rates are  $\mu_{t\bar{t}W} =$   
127  $1.43 \pm 0.21$  (stat+syst) and  $\mu_{t\bar{t}Z} = 1.03 \pm 0.14$  (stat+syst). The  $t\bar{t}Z$  production rate is in clear  
128 agreement with the model, while the  $t\bar{t}W$  production rate is slightly above the expectations. The  
129 observed (expected) significance for  $t\bar{t}H$  production is 4.7 (5.2) standard deviations, while it is 1.4  
130 (0.3) for the  $tH$  signal.

### 131 3.4 Interpretation

132 The observed yields can also be interpreted in terms of inference in the coupling modifier of  
133 the Higgs boson to the top quark ( $\kappa_t$ ) and to the W and Z bosons ( $\kappa_V$ ). The compatibility of the  
134 observed data is compared for a grid of ( $\kappa_t$ ,  $\kappa_V$ ) hypotheses, computing a likelihood score. The  
135 effect of deviations of  $\kappa_t$  and  $\kappa_V$  with respect to the unity in the kinematic distribution of  $tH$  events  
136 and the H boson branching fractions are taking into account.

137 The likelihood scan allows to construct confidence level regions in the ( $\kappa_t$ ,  $\kappa_V$ ) plane and  
138 confidence intervals in  $\kappa_t$ . The results allow to constrain  $\kappa_t$  to be within  $-0.9 < \kappa_t < -0.7$  or  
139  $0.7 < \kappa_t < 1.1$  and 95% confidence level.

### 140 4. Conclusions

141 The observation of the Yukawa interactions between the top quark and the Higgs boson are  
142 crucial to establish the validity of the SM of particle physics. These couplings can be explored at  
143 tree level by performing measurements of  $t\bar{t}H$  and  $tH$  production, which can be done with high  
144 precision in the diphoton and multilepton final states. These measurements have been performed by  
145 the CMS Collaboration and are shown in this contribution. The results obtained are consistent with  
146 the SM expectations and achieve sensitivities for  $t\bar{t}H$  production above five standard deviations.

147 The author thanks Programa Severo Ochoa del Principado de Asturias for funding this work.

### 148 References

- 149 [1] ATLAS Collaboration, *Phys.Lett.* **B 716** (2012) 1-29  
150 [2] CMS Collaboration, *JINST* **3** S08004 (2008)  
151 [3] CMS Collaboration, *Phys. Lett.* **B 716** (2012) 30  
152 [4] CMS Collaboration, *Phys. Rev. Lett.* , **125** 061801 (2020)  
153 [5] CMS Collaboration, [CMS-PAS-HIG-19-008](#)  
154 [6] CMS Collaboration, [CMS-DP-2019-033](#)  
155 [7] Alwall et al., *JHEP* **07** (2014) 079  
156 [8] Frederix, Tsinikos, *Eur. Phys. J. C* **80** (2020) 803  
157 [9] Dror et al., *JHEP* **01** (2016) 071  
158 [10] Sjöstrand et al., *Comput. Phys. Commun.* **191** (2015) 159  
159 [11] ATLAS and CMS Collaborations, ATL-PHYS-PUB-2011-011, [CMS-NOTE-2011-005](#).